ACS APPLIED MATERIALS & INTERFACES

RESEARCH ARTICLE

www.acsami.org

Effect of Self-Assembled Monolayers on Charge Injection and Transport in Poly(3-hexylthiophene)-Based Field-Effect Transistors at Different Channel Length Scales

K. A. Singh,[†] T. L. Nelson,[‡] J. A. Belot,[‡] T. M. Young,[‡] N. R. Dhumal,[‡] T. Kowalewski,[‡] R. D. McCullough,[‡] P. Nachimuthu,[§] S. Thevuthasan,[§] and L. M. Porter[*,†]

[†]Department of Materials Science and Engineering, Carnegie Mellon University, 5000 Forbes Avenue, Pittsburgh, Pennsylvania 15213, United States

[‡]Department of Chemistry, Carnegie Mellon University, 4400 Fifth Avenue, Pittsburgh, Pennsylvania 15213, United States

[§]EMSL, Pacific Northwest National Laboratory, Richland, Washington 99352, United States

Supporting Information

ABSTRACT: Charge injection and transport in bottom-contact regioregular-poly(3-hexylthiophene) (rr-P3HT) based field-effect transistors (FETs), wherein the Au source and drain contacts are modified by self-assembled monolayers (SAMs), is reported at different channel length scales. Ultraviolet photoelectron spectroscopy is used to measure the change in metal work function upon treatment with four SAMs consisting of thiol-adsorbates of different chemical composition. Treatment of FETs with electron-poor (electron-rich) SAMs resulted in an increase (decrease) in contact metal work function because of the electron-withdrawing (-donating) tendency of the polar molecules. The change in metal work function affects charge injection and is reflected in the form of the modulation of the contact resistance, R_C. For example, R_C decreased to 0.18 MΩ in the case of the (electron-poor) 3,5-bis-trifluoromethylbenzenethiol treated contacts from the value of 0.61 MΩ measured in the case of clean Au-contacts, whereas it increased to 0.97 MΩ in the case of the (electron-rich) 3-thiomethylthiophene treated contacts. Field-effect mobility values are observed to be affected in short-channel devices (<20 μm) but not in long-channel devices. This channel-length-dependent behavior of mobility is attributed to grain-boundary limited charge transport at longer channel lengths in these devices.

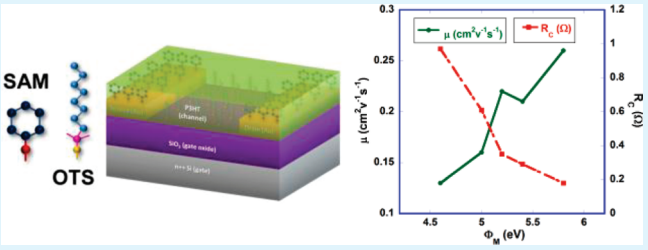

KEYWORDS: organic field effect transistors, self-assembled monolayers, photoelectron spectroscopy, charge mobility

INTRODUCTION

Organic (semi)conductors (OSCs) are poised to transform the electronics industry toward unprecedented versatility. The novel combination of electrical and mechanical properties of OSCs, and the ability to process these materials at low temperatures and cost make them particularly well-suited for large-area, flexible electronic devices.[1−4] Recent developments in the synthesis of OSCs coupled with the improvement in their morphology and dielectric−organic interfaces have further advanced the commercialization of organic electronic devices.[4,5]

A critical limitation of organic semiconductor device performance is the ability to control the charge injection at metal-contact/organic semiconductor interfaces. For example, high contact resistances ($R_C \approx 1 \times 10^4$ to 1×10^8 Ω) in organic field-effect transistors (OFETs) severely affect the device performance.[6,7] It is often observed that in devices with short channels, which are essential for fast switching speeds and lower drive currents, the contact resistance can dominate the channel resistance.[8−11] Thus, more concentrated efforts are required in order to improve the charge injection at the (metal) contact-OSC interfaces.

The contact resistance in OFETs depends on the energy level alignment between the metal contact and the (p-type) OSC in addition to the OSC morphology in the vicinity of the contacts.[10−12] The interface between an OSC, such as rr-P3HT, with a low ionization potential, and a metal, such as Au, with a high work function (Φ_M), has a finite charge injection barrier (0.3−0.7 eV) for hole injection because of the presence of an interfacial-dipole at the metal−OSC interface.[13,14] It is therefore important to reduce the barrier height for hole injection ($\Phi_{B(h)}$) to reduce the resistance of the ohmic contacts. The interfacial barrier height can be modulated by various methods. For example, depinning of the Fermi level at metal−organic interfaces using thin (∼2−6 nm) Si_3N_4 interfacial layers to produce tunneling contacts has recently been reported.[15] Other methods include changing the contact metal,[10,16] chemical treatment,[17] adding a hole injecting layer,[18] and treatment of the contacts with self-assembled monolayers (SAMs).[19−29]

Received: April 11, 2011
Accepted: July 11, 2011
Published: July 26, 2011

dx.doi.org/10.1021/am200449x | ACS Appl. Mater. Interfaces 2011, 3, 2973–2978

Self-assembled monolayers are crystalline (or semicrystalline) organic assemblies, spontaneously formed by the adsorption of molecular species onto a surface. SAMs can readily be synthesized and can be easily deposited on the devices by solution or vapor based techniques.[21,22] Treatment of the metal contacts with SAMs offers a simple and easy way to tailor charge injection and transport in OFETs as the SAMs can modify Φ_M of the contacts, thereby reducing $\Phi_{B(h)}$.[23,26,27,29]

Although there have been studies on the effect of SAM treatment of contacts in (opto)electronic devices, the physics behind changes in the interfacial barrier is still not well understood.[26,30] Making the matter more complicated, there have been reports showing minimal or, in some cases, even an opposite effect of a change in interfacial barrier upon the performance of SAM treated devices.[25,30] A number of reports suggest that the actual change in device performance is because of a change in morphology of OSCs upon SAM treatment;[25,31] whereas other reports refute this claim.[23] To clearly discern morphology changes in the active region, it would be important to distinguish between characterization of bulk or thick films and that of very thin films or regions of the film adjacent to the contacts or gate dielectric.[32]

In this study, we report on the modulation of the work function of Au electrodes by the use of electron-rich and electron-poor aromatic SAMs. The modulation of the work function of Au is measured using ultraviolet photoelectron spectroscopy (UPS). Effects on the electrical performance (contact resistance and field-effect mobility) in rr-P3HT-based FETs are reported. The effect of SAM treatment on charge transport for FETs having different channel lengths is discussed.

RESULTS AND DISCUSSION

The chemical structures of the organic molecules used to form SAMs on Au surfaces in this study are shown in Figure 1. In each of the chemical structures, the thiol group acts as the headgroup that binds to the Au surface. The first three SAMs (Figure 1a−c), viz. 3,5-bis-trifluoromethylbenzenethiol (BTFMBT), pentafluorobenzenethiol (PFBT), and 2,3,5,6-tetrafluorobenzenethiol (TFBT) molecules are electron-withdrawing in nature because of the presence of the strongly electronegative fluorine present in these molecules (and thus form "electron-poor" SAMs).[21,22] On the other hand, the 3-thiomethylthiophene (3-TMT, Figure 1d) is electron-donating in nature (and thus forms an "electron-rich" SAM). Aromatic SAMs were chosen versus aliphatic SAMs because we expect improved wettability between aromatic SAMs and the aromatic P3HT. Higher I_{on}/I_{off} ratios have also been reported for aromatic SAMs incorporated in TFTs.[24]

The presence of the SAMs on Au substrates was verified using X-ray photoelectron spectroscopy (see the Supporting Information), whereas UPS was used to determine Φ_M. Figure 2 shows UPS spectra of the clean Au substrate and the Au substrates treated with the respective SAMs. The complete spectrum is shown in Figure 2b, whereas Figure 2a and Figure 2c show the expanded view of the higher binding energy (secondary electron) and the lower binding energy (Fermi-edge) cut-offs, respectively. The work function of a sample is calculated by simply subtracting the width of its UPS spectrum from the energy of the He (I) line, which is 21.2 eV.[14,33] The width of a UPS spectrum is determined by the intersections of the linear fits of the high and low binding energy cutoffs (secondary cutoff edge and Fermi-edge respectively) with the binding energy axis.[34]

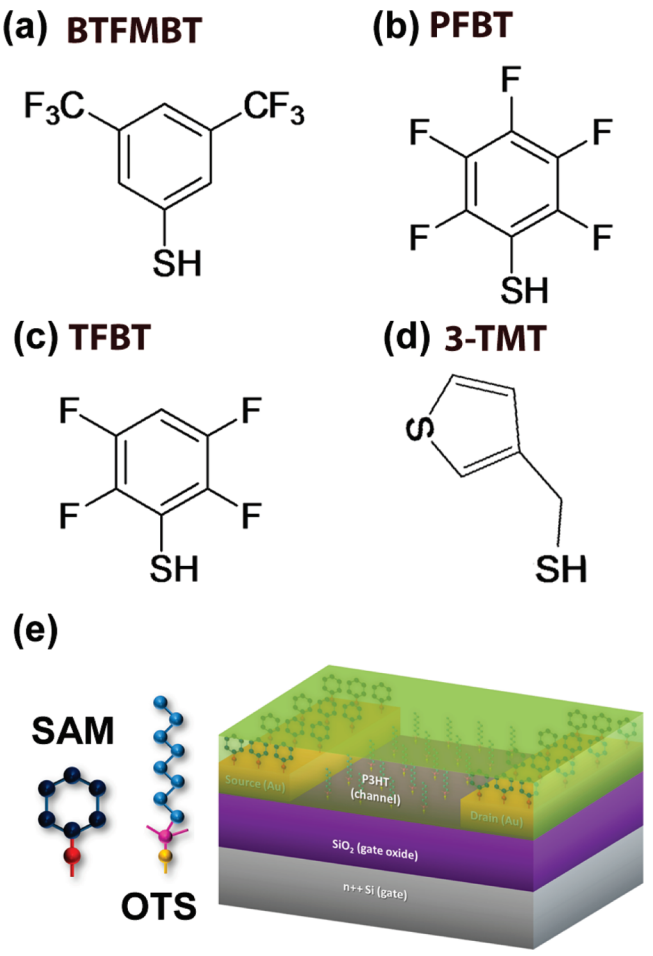

Figure 1. Chemical structures of the thiol-adsorbates used to form SAMs in this study: (a) 3,5-bis-trifluoromethylbenzenethiol; (b) pentafluorobenzenethiol; (c) 2,3,5,6-tetrafluorobenzenethiol; and (d) 3-thiomethylthiophene. A schematic of a SAM treated rr-P3HT based FET is shown in (e) with the SAM layer on Au contacts and OTS layer on SiO_2.

The work function of Au with and without the different SAMs and the dipole moments of the respective SAM molecules are listed in table 1. The dipole moments for the SAMs were calculated using the GAUSSIAN 03 program at B3LYP/6-31++G(d, p) level (For more details, see section S2 in the Supporting Information).[35] It can be observed that Φ_M displays a linear variation with the dipole moment of the thiol adsorbates. As expected, the treatment of Au with the electron-poor SAMs (1−3) increases Φ_M from its original value of 5.0 eV. TFBT and PFBT increase Φ_M to 5.2 and 5.4 eV, respectively, and BTFMBT results in the highest increase in Φ_M to 5.8 eV. In contrast the electron-rich 3-TMT molecule decreases Φ_M to 4.6 eV.

In this study, we show only the empirical relationship between the dipole moment of the SAM and Φ_M instead of calculating the expected change in Φ_M from the dipole moment values. This is because the overall change in work function, $\Delta\Phi_M$, depends upon factors like the orientation of the SAMs, their coverage density, etc., in addition to the dipole moment of the molecule itself. These calculations are widely covered in the literature and have not been included in this study.[28]

The effect of treatment of Au contacts with SAMs on the electrical performance was tested in rr-P3HT-based field-effect transistors having a bottom-contact, bottom-gate configuration

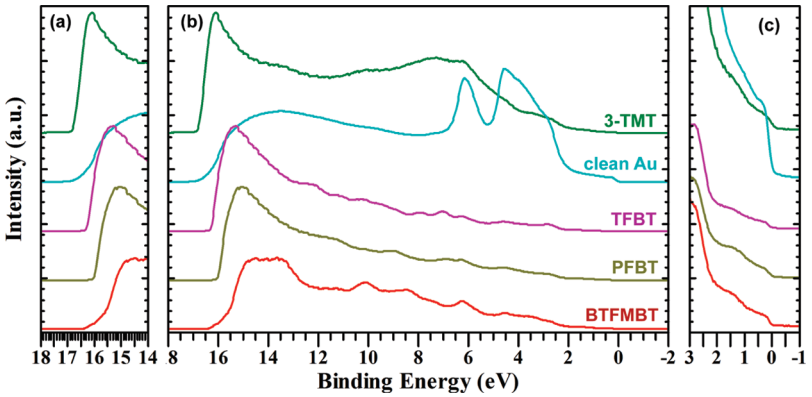

Figure 2. Ultraviolet photoelectron spectra for clean and SAM treated Au substrates: (a, c) high and low binding energy cutoff area of the spectra, respectively.

Table 1. Effect of SAMs on Contact Resistance and Work Function of Au

SAM	dipole moment of SAM (D)	Φ_M (eV)	$\Delta\Phi_M$ (eV)	R_C (MΩ)	μ ($cm^2V^{-1}s^{-1}$)
BTFMBT	+2.63	5.8	0.8	0.18	0.26
PFBT	+1.76	5.4	0.4	0.29	0.21
TFBT	+0.91	5.2	0.2	0.35	0.22
None (bare Au)	N/A	5.0		0.61	0.16
3-TMT	−1.64	4.6	−0.4	0.97	0.13

(shown in Figure 1e).[12] The devices operate as *p*-type FETs in accumulation mode.[6] The field-effect mobility was extracted in the saturation regime using the following equation:

$$\mu = \frac{2L}{WC_i}\left(\frac{\partial\sqrt{I_D}}{\partial V_G}\right)^2 \quad (1)$$

by plotting $I_D^{1/2}$ as a function of V_G (graph not shown), where W is the width of the channel, and C_i is the capacitance per unit area of the gate dielectric. R_C was extracted using the gated transmission line method for OFETs.[12,16] The slopes of the output characteristics in the linear regime (source-drain voltage, V_D = 0 to −2.5 V) were used to calculate the total device resistance values ($R_{tot} = \partial V_D/\partial I_D$). R_C values are given by the intercept of the linear fits to the plots of R_{tot} vs L.

Figure 3 shows the variation in R_C and μ as a function of Φ_M. The effect of the change in the metal work-function on the charge injection is clearly reflected by the monotonic decrease in R_C with increasing Φ_M. R_C decreases from 0.61 MΩ for clean Au contacts to 0.18 MΩ for (electron-poor) BTFMBT-treated Au contacts. Conversely, R_C increases to 0.97 MΩ in the case of (electron-rich) 3-TMT-treated Au contacts.

The modulation of contact resistance is attributed to the change in Φ_M upon SAM treatment, which should accordingly affect $\Phi_{B(h)}$. In the limiting case where we assume there is no change in the interfacial dipole between the metal and the polymer, the change in $\Phi_{B(h)}$ should equal the change in the Φ_M. However, it is reasonable to believe that introducing a layer of soft, conductive molecules between the metal and the polymer would affect the interfacial-dipole because of a reduction in the "pillow-effect" or other interfacial interactions.[14] Although we do

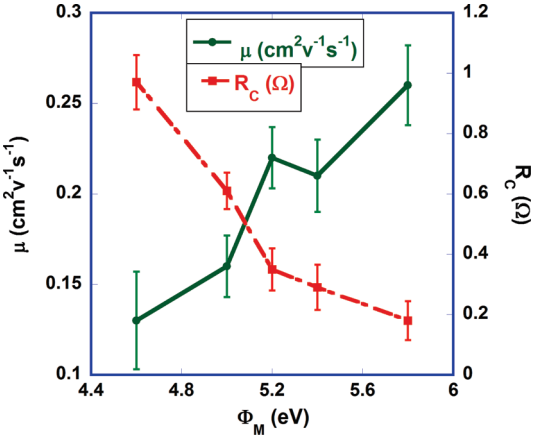

Figure 3. Field-effect mobility and contact resistance as a function of contact work function at V_G = −80 V. Mobility is reported at L = 3 μm. Each data point for mobility represents an average value of 6 devices; for contact resistance, each point represents an average of 4 sets of devices, each set having 7 different channel lengths.

not know how much $\Phi_{B(h)}$ changes with Φ_M, primarily because of the difficulty to observe the buried metal−polymer interface using UPS,[23] the change in the measured R_C values indicates that $\Phi_{B(h)}$ increases or decreases in accordance with Φ_M.

Treatment of the contacts with SAMs was also found to affect μ in short-channel (~3 μm) devices (Figure 3). For example, μ increased from 0.16 $cm^2\ V^{-1}\ s^{-1}$ for clean Au contacts to 0.26 $cm^2\ V^{-1}\ s^{-1}$ for BTFMBT-treated Au contacts. Conversely μ decreased to 0.13 $cm^2\ V^{-1}\ s^{-1}$ for 3-TMT-treated Au contacts. The inverse correlation between R_C and μ is consistent with reports in the literature highlighting the interdependence of charge injection and transport in rr-P3HT-based OFETs.[10−12,16,23]

It is possible that part of the difference in electrical performance upon SAM treatment could be associated with a change in morphology in addition to the interfacial-barrier modulation discussed above. For example, Gundlach et al.[36] reported dramatic improvements in the crystallinity of solution-cast acene-based OTFTs on contacts treated with pentafluorobenzene thiol (PFBT) SAMs and showed a corresponding increase in field-effect mobility for short-channel (L < 25 μm) devices. Better electrical performance in pentacene-based devices have also been attributed to morphological changes.[25] However, our limited

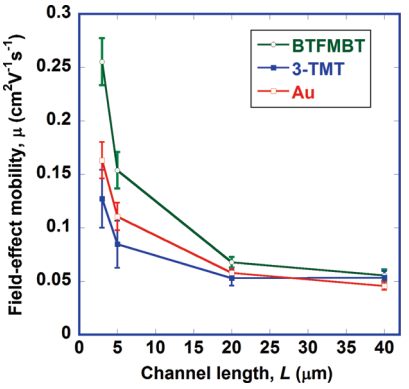

Figure 4. Variation in field-effect mobility as a function of the channel length at $V_G = -80$ V.

studies (not shown) using atomic force microscopy revealed no apparent differences in morphology of P3HT upon SAM treatment of Au contacts even for relatively thin P3HT layers. This difference may be associated with the larger size of the P3HT polymer in comparison with the other organic films.

We also believe that morphology changes would not explain the correlation between the electrical properties of our P3HT-based devices and the metal work function, or dipole moments. Additionally, a study by Hamadani et al. shows that a change in morphology alone cannot explain the difference in electrical performance[37] of rr-P3HT based OFETs upon SAM treatment.[23] They found that the current−voltage curves of electron-poor SAM-treated OFETs (unlike devices with clean Au contacts) maintain linearity and exhibit lower R_C and higher μ values upon successive dedoping of P3HT in vacuum. Obviously this result is because of the lower charge injection barrier in the case of the SAM treated device. Clearly, the effect of the change in metal work function upon SAM treatment on the electrical performance of OFETs cannot be neglected, especially in the case of devices with polymeric semiconductors like P3HT.

Figure 4 shows a plot of the variation in μ as a function of channel length for rr-P3HT based OFETs with three types of contacts: (i) clean, (ii) (electron-poor) BTFMBT-treated, and (iii) (electron-rich) 3-TMT treated Au contacts. As expected, at short channels, μ was higher in the case of BTFMBT-treated devices whereas it was lower in the case of 3-TMT-treated devices, as compared to the devices having clean Au contacts. However, the SAMs only affected μ at shorter channel lengths ($L < 20$ μm). As L increases, the mobility values decrease and become nearly equal. For example, $\mu \approx 0.05$ cm^2 V^{-1} s^{-1} at $L =$ 40 μm for the devices regardless of surface treatment.

The inverse channel length dependence of μ has been reported previously in the literature.[11,37,38] In the absence of detailed knowledge of polymer morphology across the channel, a Poole−Frenkel (PF) effect is often invoked to explain the observed behavior.[37,38] While this model results in oversimplification and does not take into account nonuniformities across the channel,[39,40] it provides a useful departure point for analysis in this study. According to Poole−Frenkel theory, μ is predicted to depend on the source−drain electric field, E_{S-D} as follows:

$$\mu = \mu_0 \exp(\gamma \sqrt{E_{S-D}}) \quad (2)$$

where μ_0 is the zero-field mobility, γ is a prefactor depending on temperature, and $E_{S\text{-}D}$ is the electric field between the source and the drain contacts.[41] It follows from the equation above that μ varies inversely with L as it is assumed that $E_{S-D} = V_{S-D}/L$, where V_{S-D} is the potential drop across the channel length L.[37,42]

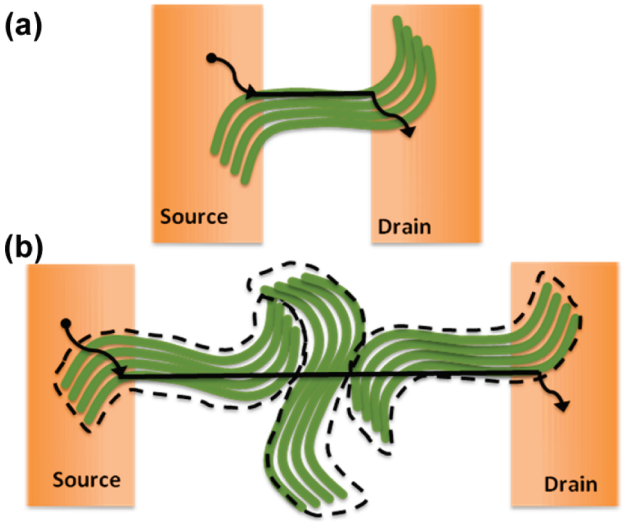

Figure 5. Schematic showing (a) bridging P3HT nanofibrils at shorter channel lengths and (b) grain boundary limited charge transport at longer channel lengths. The solid black line signifies the charge transport along the direction of the source-drain electric field in both the cases. The boundaries of the crystalline domains of rr-P3HT have been marked by the broken curves. Noncrystalline domains have not been shown.

Applying this theory in our case, the treatment of the devices with SAMs should change the potential drop across the interface and, thereby affect E_{S-D} in the three cases. In the case of the electron-poor SAM-treated devices, the decrease in the interfacial charge injection barrier results in higher E_{S-D} and thereby higher μ. On the other hand, in the case of an electron-rich SAM-treated device the higher potential drop at the contacts should mask the PF effect thereby resulting in lower dependence of L on μ.

However, if we take the effect of the rr-P3HT morphology on the charge transport into consideration then we can argue that one of the contributing factors for the channel length dependence of field-effect mobility is the extension (or lack of it) of the rr-P3HT nanofibrils (ribbonlike structures formed by lateral stacking of rr-P3HT chains, see the Supporting Information) across the length of the channel as schematically shown in Figure 5.[11,12,43] We studied this behavior in detail in a recent study, wherein we observed similar charge injection and transport behavior upon modification of the contacts by recessing them into the gate dielectric to get a planar OFET configuration.[11] Large area morphology studies of rr-P3HT in short and long channel OFETs demonstrated that for short channels ($L < 20$ μm) some rr-P3HT nanofibrils can span the entire channel length. In short-channel devices, fast charge transport is expected to occur along the channel-spanning fibrils. On the other hand, this advantage is not present in long-channel devices wherein μ is limited by the resistance of grain boundaries in the channel. This observation is consistent with the lack of improvement in field-effect mobility upon SAM treatment in long-channel devices. As such, the channel lengths at which mobility values are reported must be considered.

CONCLUSIONS

In summary, the work function of Au surfaces was modulated by treating them with electron-rich and electron-poor self-assembled

monolayers of aromatic thiols. Electron-poor (electron-rich) SAMs resulted in an increase (decrease) in the Au work function because of the electron-withdrawing (-donating) tendency of the polar molecules. The change in metal work function in turn affects charge injection reflected in the form of the modulation of the contact resistance. While there was a clear effect on charge injection, mobility values improved only in the short-channel (<20 μm) devices, indicating that charge transport in long-channel OFETs is grain-boundary (channel) limited. Our results, while reconfirming the effect of SAMs on charge injection and transport, show that it is important to take into consideration the channel length of the devices. This is specifically important in the case of a semicrystalline (or amorphous) polymeric system like rr-P3HT. The results of this study indicate that the treatment of metallic contacts using selected SAMs is beneficial in devices with short channels.

EXPERIMENTAL SECTION

Sample Preparation for Photoelectron Spectroscopy. The starting substrate was a highly doped (n+) Si wafer. The wafers were etched with buffered oxide etchant (BOE) to remove the oxide layer. Thereafter 5 nm of Ti (adhesion layer) and 50 nm of Au were sputtered onto the n+ Si wafer. The wafers were then diced into square pieces with side dimension = 2 cm. PFBT, TFBT and BTFMBT were purchased from Sigma-Aldrich and used without further purification. 3-TMT was synthesized and purified according to the reported literature.[44,45] The samples were dipped in the SAM solution (prepared in absolute ethanol at a concentration of 10 mM) for 2 h before introduction into the chamber for photoemission measurements.

Photoelectron Spectroscopy Measurements. The photoemission measurements were conducted using a Phi 5000 VersaProbe (Scanning ESCA Microprobe) system located at the EMSL, Pacific Northwest National Laboratory. This system consists of a monochromatic focused Al K_α X-ray (1486.7 eV) source, a He source and a hemispherical analyzer.

UPS measurements were conducted using the He I ($h\nu$ = 21.2 eV) line and a pass-energy of 0.585 eV. During UPS measurements −7.0 V bias was applied to the sample in order to separate the sample and analyzer high binding energy cutoffs. The photoelectrons were collected from the sample surface normal to the analyzer. The instrumental broadening was found to be 0.26 eV according to the method mentioned by Schlaf et al.[34] Therefore, to account for the 0.26 eV broadening, 0.13 eV was subtracted from the higher binding energy cutoff and the same value was added to the lower binding energy cutoff to derive the final Φ_M values. The photoelectron spectroscopy data was analyzed using CasaXPS.

Field-Effect Transistor Fabrication. The OFETs were fabricated on a degenerately doped (n+) Si wafer having a 250 nm SiO_2 layer on top acting as the gate dielectric layer. A layer of positive photoresist was spun at 4000 rpm onto the wafer and exposed to UV light to pattern the source and the drain contact areas. Electron beam evaporation in an ultrahigh vacuum chamber was subsequently used to deposit a 3 nm-thick Ti adhesion layer followed by deposition of ∼47 nm Au layer to get the desired contact height of 50 nm. The photoresist was then stripped using lift-off in an ultrasonic bath containing acetone. The devices were cleaned in an oxygen-plasma at 300 W for 20 min so as to remove organic residue that may have remained after the photolithographic process. The channel width, W, of the OFETs was kept fixed at 250 μm whereas the channel length, L, was varied from 3 to 40 μm. Regioregular-P3HT (weight average molecular weight, M_W = 18 kDa; poly dispersity index (PDI) = 1.1) was synthesized in-house as described earlier.[46,47] Prior to polymer deposition the devices were cleaned for 20 min at 120 °C using UV-ozone. The devices were then surface treated in a 30 mM solution of octyltrichlorosilane in hexadecane under a N_2 atmosphere to make the substrate surface hydrophobic. Thereafter, the devices were treated with the aromatic thiol solutions to form SAMs on the contacts just like in the case of substrate preparation for photoelectron spectroscopy measurements. The devices were then sonicated in absolute ethanol for 10 min before drying them at 150 °C in N_2 followed by vacuum storage for 2 h. Polymer films were then deposited from a 1 mg mL^{-1} rr-P3HT solution in chloroform using the solvent-assisted drop-casting method.[12]

Current−Voltage Measurements. After polymer deposition the OFETs were kept under vacuum (∼ 20 mbar) for 24−48 h prior to electrical measurements. The current−voltage characteristics were recorded using an Agilent 4155C semiconductor parameter analyzer. The devices were kept in the dark and under a flow of argon gas during the measurements.

ASSOCIATED CONTENT

Supporting Information. Additional figures and information (PDF). This material is available free of charge via the Internet at http://pubs.acs.org.

AUTHOR INFORMATION

Corresponding Author
*E-mail: lporter@andrew.cmu.edu.

ACKNOWLEDGMENT

Research funding from the National Science Foundation (Grant #'s ECS0524340 and ECCS0824188) and the Pennsylvania Infrastructure Technology Alliance is gratefully acknowledged. A portion of the research was performed using EMSL, a national scientific user facility sponsored by the Department of Energy's Office of Biological and Environmental Research and located at Pacific Northwest National Laboratory.

REFERENCES

(1) Clemens, W.; Fix, I.; Ficker, J.; Knobloch, A.; Ullmann, A. *J. Mater. Res.* **2004**, *19*, 1963–1973.
(2) Bao, Z. N. *Adv. Mater.* **2000**, *12*, 227–230.
(3) *Organic Electronics: Materials, Manufacturing and Applications*; Klauk, H., Ed.; WILEY-VCH Verlag GmbH & Co. KGaA: Weinheim, Germany, 2006.
(4) Katz, H. E.; Huang, J. *Annu. Rev. Mater. Res.* **2009**, *39*, 71–92.
(5) Osaka, I.; McCullough, R. D. *Acc. Chem. Res.* **2008**, *41*, 1202–1214.
(6) Horowitz, G. *Adv. Mater.* **1998**, *10*, 365–377.
(7) Sirringhaus, H. *Adv. Mater.* **2005**, *17*, 2411–2425.
(8) Meijer, E. J.; Gelinck, G. H.; van Veenendaal, E.; Huisman, B. H.; de Leeuw, D. M.; Klapwijk, T. M. *Appl. Phys. Lett.* **2003**, *82*, 4576–4578.
(9) Hamadani, B. H.; Natelson, D. *Appl. Phys. Lett.* **2004**, *84*, 443–445.
(10) Burgi, L.; Richards, T. J.; Friend, R. H.; Sirringhaus, H. *J. Appl. Phys.* **2003**, *94*, 6129–6137.
(11) Singh, K. A.; Young, T.; McCullough, R. D.; Kowalewski, T.; Porter, L. M. *Adv. Funct. Mater.* **2010**, *20*, 2216–2221.
(12) Singh, K. A.; Sauve, G.; Zhang, R.; Kowalewski, T.; McCullough, R. D.; Porter, L. M. *Appl. Phys. Lett.* **2008**, *92*, 263303.
(13) Hirose, Y.; Kahn, A.; Aristov, V.; Soukiassian, P.; Bulovic, V.; Forrest, S. R. *Phys. Rev. B* **1996**, *54*, 13748–13758.
(14) Hwang, J.; Wan, A.; Kahn, A. *Mater. Sci. Eng., R* **2009**, *64*, 1–31.
(15) Liu, Z. H.; Kobayashi, M.; Paul, B. C.; Bao, Z. N.; Nishi, Y. *Phys. Rev. B* **2010**, *82*, 035311.
(16) Hamadani, B. H.; Natelson, D. *J. Appl. Phys.* **2005**, *97*, 064508.

(17) Stadlober, B.; Haas, U.; Gold, H.; Haase, A.; Jakopic, G.; Leising, G.; Koch, N.; Rentenberger, S.; Zojer, E. *Adv. Funct. Mater.* **2007**, *17*, 2687–2692.
(18) Hong, K.; Yang, S. Y.; Yang, C.; Kim, S. H.; Choi, D.; Park, C. E. *Org. Electron.* **2008**, *9*, 864–868.
(19) Campbell, I. H.; Kress, J. D.; Martin, R. L.; Smith, D. L.; Barashkov, N. N.; Ferraris, J. P. *Appl. Phys. Lett.* **1997**, *71*, 3528–3530.
(20) Khodabakhsh, S.; Poplavskyy, D.; Heutz, S.; Nelson, J.; Bradley, D. D. C.; Murata, F.; Jones, T. S. *Adv. Funct. Mater.* **2004**, *14*, 1205–1210.
(21) Ulman, A. *An Introduction to Ultrathin Organic Films from Langmuir-Blodgett to Self-Assembly*; Academic Press: San Diego, CA, 1991.
(22) Love, J. C.; Estroff, L. A.; Kriebel, J. K.; Nuzzo, R. G.; Whitesides, G. M. *Chem. Rev.* **2005**, *105*, 1103–1169.
(23) Hamadani, B. H.; Corley, D. A.; Ciszek, J. W.; Tour, J. M.; Natelson, D. *Nano Lett.* **2006**, *6*, 1303–1306.
(24) DiBenedetto, S. A.; Facchetti, A.; Ratner, M. A.; Marks, T. J. *Adv. Mater.* **2009**, *21*, 1407–1433.
(25) Asadi, K.; Wu, Y.; Gholamrezaie, F.; Rudolf, P.; Blom, P. W. M. *Adv. Mater.* **2009**, *21*, 4109–4114.
(26) Rissner, F.; Rangger, G. M.; Hofmann, O. T.; Track, A. M.; Heimel, G.; Zojer, E. *ACS Nano* **2009**, *3*, 3513–3520.
(27) de Boer, B.; Hadipour, A.; Mandoc, M. M.; van Woudenbergh, T.; Blom, P. W. M. *Adv. Mater.* **2005**, *17*, 621–625.
(28) Alloway, D. M.; Hofmann, M.; Smith, D. L.; Gruhn, N. E.; Graham, A. L.; Colorado, R.; Wysocki, V. H.; Lee, T. R.; Lee, P. A.; Armstrong, N. R. *J. Phys. Chem. B* **2003**, *107*, 11690–11699.
(29) Zehner, R. W.; Parsons, B. F.; Hsung, R. P.; Sita, L. R. *Langmuir* **1999**, *15*, 1121–1127.
(30) Cheng, X.; Noh, Y.-Y.; Wang, J.; Tello, M.; Frisch, J.; Blum, R.-P.; Vollmer, A.; Rabe, J. P.; Koch, N.; Sirringhaus, H. *Adv. Funct. Mater.* **2009**, *19*, 2407–2415.
(31) Chen, W.; Gao, X. Y.; Qi, D. C.; Chen, S.; Chen, Z. K.; Wee, A. T. S. *Adv. Funct. Mater.* **2007**, *17*, 1339–1344.
(32) Kline, R. J.; Mcgehee, M. D.; Toney, M. F. *Nat. Mater.* **2006**, *5*, 222–228.
(33) Alloway, D. M.; Graham, A. L.; Yang, X.; Mudalige, A.; Colorado, R.; Wysocki, V. H.; Pemberton, J. E.; Lee, T. R.; Wysocki, R. J.; Armstrong, N. R. *J. Phys. Chem. C* **2009**, *113*, 20328–20334.
(34) Schlaf, R.; Schroeder, P. G.; Nelson, M. W.; Parkinson, B. A.; Lee, P. A.; Nebesny, K. W.; Armstrong, N. R. *J. Appl. Phys.* **1999**, *86*, 1499–1509.
(35) Frisch, M. J.; Trucks, G. W.; Schlegel, H. B.; Scuseria, G. E.; Robb, M. A.; Cheeseman, J. R.; Montgomery, J. A., Jr.; Vreven, T.; Kudin, K. N.; Burant, J. C.; Millam, J. M.; Iyengar, S. S.; Tomasi, J.; Barone, V.; Mennucci, B.; Cossi, M.; Scalmani, G.; Rega, N.; Petersson, G. A.; Nakatsuji, H.; Hada, M.; Ehara, M.; Toyota, K.; Fukuda, R.; Hasegawa, J.; Ishida, M.; Nakajima, T.; Honda, Y.; Kitao, O.; Nakai, H.; Klene, M.; Li, X.; Knox, J. E.; Hratchian, H. P.; Cross, J. B.; Bakken, V.; Adamo, C.; Jaramillo, J.; Gomperts, R.; Stratmann, R. E.; Yazyev, O.; Austin, A. J.; Cammi, R.; Pomelli, C.; Ochterski, J. W.; Ayala, P. Y.; Morokuma, K.; Voth, G. A.; Salvador, P.; Dannenberg, J. J.; Zakrzewski, V. G.; Dapprich, S.; Daniels, A. D.; Strain, M. C.; Farkas, O.; Malick, D. K.; Rabuck, A. D.; Raghavachari, K.; Foresman, J. B.; Ortiz, J. V.; Cui, Q.; Baboul, A. G.; Clifford, S.; Cioslowski, J.; Stefanov, B. B.; Liu, G.; Liashenko, A.; Piskorz, P.; Komaromi, I.; Martin, R. L.; Fox, D. J.; Keith, T.; Al-Laham, M. A.; Peng, C. Y.; Nanayakkara, A.; Challacombe, M.; Gill, P. M. W.; Johnson, B.; Chen, W.; Wong, M. W.; Gonzalez, C.; Pople, J. A. *Gaussian 03*, revision D.01; Gaussian, Inc.: Wallingford, CT, 2004.
(36) Gundlach, D. J.; Royer, J. E.; Park, S. K.; Subramanian, S.; Jurchescu, O. D.; Hamadani, B. H.; Moad, A. J.; Kline, R. J.; Teague, L. C.; Kirillov, O.; Richter, C. A.; Kushmerick, J. G.; Richter, L. J.; Parkin, S. R.; Jackson, T. N.; Anthony, J. E. *Nat. Mater.* **2008**, *7*, 216–221.
(37) Hamadani, B. H.; Richter, C. A.; Gundlach, D. J.; Kline, R. J.; McCulloch, I.; Heeney, M. *J. Appl. Phys.* **2007**, *102*, 044503.
(38) Hamadani, B. H.; Gundlach, D. J.; McCulloch, I.; Heeney, M. *Appl. Phys. Lett.* **2007**, *91*, 3.
(39) Burgi, L.; Friend, R. H.; Sirringhaus, H. *Appl. Phys. Lett.* **2003**, *82*, 1482–1484.
(40) Salleo, A.; Kline, R. J.; DeLongchamp, D. M.; Chabinyc, M. L. *Adv. Mater.* **2010**, *22*, 3812–3838.
(41) Blom, P. W. M.; deJong, M. J. M.; vanMunster, M. G. *Phys. Rev. B* **1997**, *55*, R656–R659.
(42) Frenkel, J. *Phys. Rev.* **1938**, *54*, 647–648.
(43) Zhang, R.; Li, B.; Iovu, M. C.; Jeffries-El, M.; Sauve, G.; Cooper, J.; Jia, S. J.; Tristram-Nagle, S.; Smilgies, D. M.; Lambeth, D. N.; McCullough, R. D.; Kowalewski, T. *J. Am. Chem. Soc.* **2006**, *128*, 3480–3481.
(44) Bjornholm, T.; Greve, D. R.; Reitzel, N.; Hassenkam, T.; Kjaer, K.; Howes, P. B.; Larsen, N. B.; Bogelund, J.; Jayaraman, M.; Ewbank, P. C.; McCullough, R. D. *J. Am. Chem. Soc.* **1998**, *120*, 7643–7644.
(45) Nelson, T. L. Ph.D, University of South Carolina, Columbia, SC, 2007.
(46) Loewe, R. S.; Khersonsky, S. M.; McCullough, R. D. *Adv. Mater.* **1999**, *11*, 250–253.
(47) Loewe, R. S.; Ewbank, P. C.; Liu, J. S.; Zhai, L.; McCullough, R. D. *Macromolecules* **2001**, *34*, 4324–4333.